Available online at www.sciencedirect.com
SCIENCE DIRECT®
Journal of Sound and Vibration 275 (2004) 391–413
JOURNAL OF SOUND AND VIBRATION
www.elsevier.com/locate/jsvi

Estimation of acoustic source strength within a cylindrical duct by inverse methods

Y. Kim*, P.A. Nelson

Institute of Sound and Vibration Research, University of Southampton, Southampton SO17 1BJ, UK

Received 5 March 2003; accepted 17 June 2003

Abstract

One method for deducing the strength of an acoustic source distribution from measurements of the radiated field involves the inversion of the matrix of frequency response functions relating the field measurement points to the strengths of a number of point sources used to represent the source distribution. This method uses the *singular value decomposition* (SVD) as the primary analysis tool and has shown some promise. In the transformation process associated with the SVD, the strength of the discretized point source can be simply represented by the pressure field and the inversion of corresponding matrix of the frequency response function and the transformed pressures and source distribution are related by single real numbers only (i.e., the singular values). Therefore, the resolution and the accuracy of the reconstruction produced by such inversion methods will be highly dependent on how these small singular values are treated during the inversion process. In the present work, the emphasis is placed on the description of the inverse method for the investigation of the characteristics of acoustic sources within a circular duct. Firstly, an analytical model is developed of the internal field from a finite duct with open ends. An examination is presented of the capability of the inverse method in dealing with in-duct sound source problems. These guide the design of an optimal sensor array which can make the condition number as small as possible for the assumed source distribution. Also, a series of experimental demonstrations are given of the proposed in-duct sensor array for producing high-resolution information regarding in-duct sources.

1. Introduction

The results presented in Refs. [1–4] have demonstrated the spatial resolution and the accuracy of source strength reconstruction by the application of singular value decomposition (SVD) based

*Corresponding author. Present address: Samsung Advanced Institute of Technology (SAIT), Giheung-eup, Yongin-si, Gyeonggi-do 449-712, South Korea. Tel.: +82-31-2808146; fax: +82-31-2809158.
E-mail address: ykim65@dreamwiz.com (Y. Kim).

0022-460X/$ - see front matter © 2003 Elsevier Ltd. All rights reserved.
doi:10.1016/j.jsv.2003.06.032

on an assumed source model. The usefulness of this decomposition stems from the fact that the SVD can be interpreted in terms of spatial frequency. However, in practice, as described in these references, regularization is necessary to avoid unstable solutions dominated by the errors associated with the small singular values in the acoustical frequency response function matrix.

Based on these previous results, this paper applies the inverse method to an initial investigation of the characteristics of in-duct source distributions with a view to their ultimate application to aeroacoustic sources such as those associated with the fan of a gas turbine. It would be extremely beneficial for purposes of noise control design to have information regarding the separate amplitude and phase of each source component which constitutes such a complex source distribution.

According to Refs. [5,6], a major source of noise in a ducted fan is the interaction of the blades with a non-uniform inlet flow, resulting in a dipole-like acoustic source distribution over the plane of the blades. A monopole source distribution is equivalent to the periodic introduction of mass in the source plane and simulates the effect of the blade thickness in sound generation by the ducted fan. Therefore, a sound generator such as a ducted axial fan can be simulated by a distribution of elemental acoustic sources over a cross-section of the duct. The acoustic pressure generated by a source distribution within a cylindrical duct can be expressed as the superposition of component sound waves, which are called "spinning modes" [7–9]. Some of the modes, depending on the frequency, decay exponentially, and the remainder of the spinning modes propagate along the duct and produce a radiated sound field. Each higher order spinning mode in the duct fails to propagate if the frequency falls below the "cut-off frequency". Therefore, in this paper expressions are developed for the acoustic pressure generated by a source distribution in a finite duct. It will firstly be assumed that the objective is to provide a good reconstruction of monopole sources distributed over a duct cross-section, even though it is appreciated that a dipole source model may be more appropriate to the study of fan noise.

Following the formulation for freefield sound source problems described in Refs. [1–4], when a real source is modelled by N discrete acoustic sources, the output sensed at M discrete internal field points on the duct walls can be represented by using the frequency response function matrix $\mathbf{G}_D$. This represents the matrix of complex frequency response functions relating the model acoustic pressures $\mathbf{p}$ to the model complex source strengths $\mathbf{q}$, which can be expressed as

$$\hat{\mathbf{p}} = \mathbf{G}_D\mathbf{q} + \mathbf{e}, \tag{1}$$

where $\hat{\mathbf{p}}$ denotes the M-dimensional complex vector of the measured acoustic pressures within the duct and $\mathbf{q}$ represents the N-dimensional complex vector of the acoustic source strengths assumed. It is also assumed that the difference between the model pressure $\mathbf{p}$ and the measured pressures $\hat{\mathbf{p}}$, which is caused by various kinds of errors, is expressed as the vector of complex errors given by $\mathbf{e} = \hat{\mathbf{p}} - \mathbf{p}(= \hat{\mathbf{p}} - \mathbf{G}_D\mathbf{q})$. The estimate of the acoustic source strengths, which is provided by the minimization of the sum of the squared moduli of the complex errors given by the quadratic cost function $J = \mathbf{e}^{\mathrm{H}}\mathbf{e}$, can be written as

$$\mathbf{q} = [\mathbf{G}_D^{\mathrm{H}}\mathbf{G}_D]^{-1}\mathbf{G}_D^{\mathrm{H}}\hat{\mathbf{p}}, \tag{2}$$

where the superscript H denotes the Hermitian transpose (complex conjugate transpose).

In practice, since ill-conditioning of the matrix $\mathbf{G}_D$ is almost inevitable, and thus will often result in an ill-posed problem, successful reconstruction of the acoustic source distribution cannot

always be provided by using only the simple least-squares estimation (i.e., Eq. (2)). Hence, most numerical methods for treating the ill-posed problem seek to overcome the problem associated with the ill-conditioning of the matrix. In such cases, the solution of the problem approximates the desired solution and, in addition, is a more satisfactory solution than the least-squares solution. This can be achieved by incorporating additional constraints to the desired solution, and such numerical treatments are called *regularization methods*, and they always include a regularization parameter which controls the amount of regularization. In this paper, Tikhonov regularization [10,11], one of a number of regularization methods is introduced in order to enhance the reconstruction accuracy and its spatial resolution. By the application of Tikhonov regularization, the general form of the estimate of the acoustic source strength is written as

$$\mathbf{q}_R = \left[(\mathbf{G}_D^{\mathrm{H}}\mathbf{G}_D + \beta\mathbf{I})^{-1}\mathbf{G}_D^{\mathrm{H}}\right]\hat{\mathbf{p}}, \tag{3}$$

where the subscript R denotes regularized solution and β denotes the chosen Tikhonov regularization parameter.

This paper illustrates the capability of the inverse method in producing a successful estimate of acoustic source strengths from measurements made of the radiated field within a cylindrical duct. In order to improve the spatial resolution and the accuracy of the estimation of the acoustic source distribution within the duct, this paper suggests methods for improving the conditioning of the frequency response function matrix $\mathbf{G}_D$. The suggested guidelines are demonstrated in practice under laboratory conditions and the results presented will show that the inverse technique has some potential for dealing with this kind of the problem. The capabilities of two regularization parameter-determination methods, *generalized cross-validation* (GCV) [12,13] and the *L-curve method* [14,15], examined in detail in Refs. [2,4] will also be experimentally demonstrated.

2. Model of in-duct sound transmission and radiation

2.1. The acoustic pressure field in a finite cylindrical duct

A hard-wall cylindrical duct is considered, which contains a set of point monopole sources (which are assumed here to be stationary) with the co-ordinate system illustrated in Fig. 1. It is assumed that there is no flow. The duct is of constant circular cross-section S with the radius R_d. Reflections are allowed at both ends which are open and unflanged. When harmonic time dependence is assumed such that $p(r,\theta,z,t) = \mathrm{Re}\{p(r,\theta,z)\mathrm{e}^{\mathrm{j}\omega t}\}$, the acoustic pressure field within

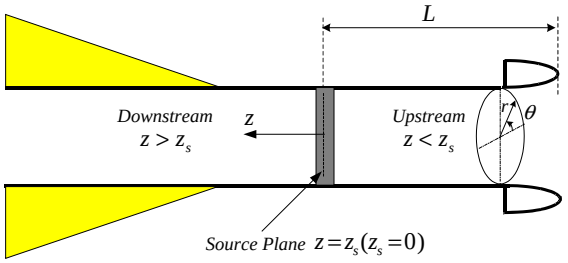

Fig. 1. A finite cylindrical duct with an acoustic source distribution.

the duct must satisfy the wave equation. This is given by

$$(\nabla^2 + k^2)p(r,\theta,z) = 0, \tag{4}$$

where $k = \omega/c_o$, ω is the angular frequency and c_o is the sound speed. The solution of Eq. (4) can be conventionally expressed by a series of spinning modes. This can be written as [7,8]

$$p(r,\theta,z) = \sum_{m=-\infty}^{\infty} \sum_{n=1}^{\infty} b_{mn}(z)\psi_{mn}(r,\theta), \tag{5}$$

where the indices m and n refer, respectively, to the azimuthal and the radial order of the spinning mode. The general form of $b_{mn}(z)$ for each mode allows for reflected waves and can be written as

$$b_{mn}(z) = A_{mn}\,\mathrm{e}^{-\mathrm{j}k_{mn}^{z+}z} + B_{mn}\,\mathrm{e}^{-\mathrm{j}k_{mn}^{z-}z}, \tag{6}$$

where the unknown constants A_{mn} and B_{mn} are the complex mode amplitudes of the forward (k_{mn}^{z+}) and backward (k_{mn}^{z-}) propagating modes, respectively. In Eq. (5), the cylindrical mode shape function $\psi_{mn}(r,\theta)$ is given by

$$\psi_{mn}(r,\theta) = \frac{\mathrm{J}_m(k_{mn}^r r)}{N_{mn}}\mathrm{e}^{-\mathrm{j}m\theta}, \tag{7}$$

where J_m is the Bessel function of the first kind of integer order m. The radial wavenumber k_{mn}^r is determined by the hard-wall boundary condition (i.e., $(\mathrm{d}p/\mathrm{d}r)|_{r=R_d} = 0$) and thus results in the following condition given by

$$k_{mn}^r \mathrm{J}'_m(k_{mn}^r R_d) = 0, \tag{8}$$

where the prime represents the first derivative of the Bessel function. The mode shape functions $\psi_{mn}(r,\theta)$ defined by Eq. (7) are orthogonal [16], such that

$$\int_S \psi_{mn}(r,\theta)\psi_{ab}^*(r,\theta)\,\mathrm{d}S = \begin{cases} 1, & \text{for } m = a, n = b, \\ 0, & \text{for } m \neq a, n \neq b. \end{cases} \tag{9}$$

Substituting the above relationships into Eq. (7) then shows that the normalizing coefficient N_{mn} is determined by

$$N_{mn}^2 = \int_S \mathrm{J}_m^2(k_{mn}^r r)\,\mathrm{d}S. \tag{10}$$

Meanwhile, for any given m, there are infinitely many values of $k_{mn}^r R_d$ that satisfy Eq. (8), and these are given by the zeros of the Bessel function derivative, $\mathrm{J}'_m(k_{mn}^r R_d)$. However, only a finite number of modes can propagate and carry acoustic energy. These are associated with real axial wavenumbers $k_{mn}^{z\pm}$. For example, substitution of the solution for the acoustic pressure field given by Eq. (5) into the wave Eq. (4) results in the following relationship between the axial and the radial wavenumbers, $k_{mn}^{z\pm}$ and k_{mn}^r [4,16]:

$$k_{mn}^{z\pm} = \pm\sqrt{k^2 - (k_{mn}^r)^2}. \tag{11}$$

From the above relationship, if k_{mn}^r is larger than k (here, the axial wavenumber $k_{mn}^{z\pm}$ will be purely imaginary), then the acoustic pressure in Eq. (5) will decay exponentially. Otherwise, there are a finite number of modes that can propagate within the duct even though the acoustic field may be described as an infinite series of modes. Hence, there exists a maximum value of k_{mn}^r such

that the axial wavenumber $k_{mn}^{z\pm}$ remains real. This is usually termed the *cut-off* property for a given mode, which is defined by $k_{mn}^{z\pm} = 0$.

The analysis presented above provides a framework which is very similar to that based on the Fourier-based techniques described in Ref. [4] for dealing with the sound radiation problems in a free field. For example, similar to the case for *nearfield acoustical holography* (NAH) [17–20], radiated modes within a duct either propagate or decay exponentially with magnitude of the axial wavenumber $k_{mn}^{z\pm}$. Hence, in order to realize high-resolution information about in-duct acoustic sources, the evanescent modes within the duct must be considered. Thus, it is very interesting to examine the acoustical in-duct inverse source problem of using field data within the duct in order to obtain an image of the source distribution. Use will be made of the general transformation process associated with the SVD described in Refs. [1–4]. Therefore, an attempt will be made to make the connection between the use of the SVD and the spatial resolution of the reconstructed source image. This has been established in a limited number of cases [16,21], but the following sections will investigate further the potential for the practical use of the SVD and provide more fully the physical interpretation of the SVD when applied to in-duct inverse source problems.

2.2. The Green function for a finite cylindrical duct

In order to determine the mode amplitudes A_{mn} and B_{mn} in Eq. (6), it is necessary to define the appropriate Green function which links the radiated pressures to the acoustic source within a cylindrical duct. Here, the Green function for a finite duct is denoted by $G(\mathbf{x}|\mathbf{y})$ and is assumed to be of a similar form to the expression given by Eq. (5) for the pressure within a duct. Thus, the Green function can be written as

$$G(\mathbf{x}|\mathbf{y}) = \sum_{m=-\infty}^{\infty} \sum_{n=1}^{\infty} b_{mn}(z)\psi_{mn}(r,\theta), \tag{12}$$

where the field point is denoted by the vector $\mathbf{x}(r,\theta,z)$ and the source position is denoted similarly by $\mathbf{y}(r_s,\theta_s,z_s)$. A general form of $b_{mn}(z)$ for each mode is given by Eq. (6). Here, the axial wavenumbers k_{mn}^{z+} and k_{mn}^{z-} correspond to forward propagating waves and backward propagating waves, respectively, and these are determined by the relation with the radial wavenumber for each mode, which is given by Eq. (11).

Now, it is necessary to present $b_{mn}(z)$ in a form suitable for Eq. (12). The complex ratio $B_{mn}^{\pm}\,\mathrm{e}^{-\mathrm{j}k_{mn}^{z-}z}/A_{mn}^{\pm}\,\mathrm{e}^{-\mathrm{j}k_{mn}^{z+}z}$ called the *reflection factor*, by using the *reflection phase* $\eta(z)$, whose value at any axial position z is defined by

$$\frac{B_{mn}^{\pm}\,\mathrm{e}^{-\mathrm{j}k_{mn}^{z-}z}}{A_{mn}^{\pm}\,\mathrm{e}^{-\mathrm{j}k_{mn}^{z+}z}} = \mathrm{e}^{2\mathrm{j}\eta_{mn}^{\pm}(z)}. \tag{13}$$

and the reflection factor at $z = 0$, which is called the *reflection coefficient* (i.e., B_{mn}/A_{mn}), can be written as

$$\frac{B_{mn}^{\pm}}{A_{mn}^{\pm}} = \mathrm{e}^{2\mathrm{j}\eta_{mn}^{0\pm}}, \tag{14}$$

where the superscripts $\pm$ for the unknown amplitudes, $A_{mn}^{\pm}$ and $B_{mn}^{\pm}$, and the reflection phase $\eta_{mn}^{\pm}(z)$ refer to the regions, respectively, downstream ($z > z_s$) and upstream ($z < z_s$) of the source at

$z = z_s$. Thus, the final form of the reflection phase $\eta_{mn}^{\pm}(z)$ for each mode at any axial position z becomes

$$\eta_{mn}^{\pm}(z) = \eta_{mn}^{0\pm} + k_{mn}z, \tag{15}$$

where $k_{mn} = \sqrt{k^2 - (k_{mn}^r)^2}$. Then, substituting Eqs. (13) and (14) into the expression for $b_{mn}(z)$ given by Eq. (6) shows [4] that

$$b_{mn}^{\pm}(z) = 2A_{mn}^{\pm}\, e^{j\eta_{mn}^{0\pm}} \cos(\eta_{mn}^{\pm}(z)). \tag{16}$$

In order to find the general form of $b_{mn}^{\pm}(z)$ at any axial position z, a ratio of $b_{mn}^{\pm}(z)$ at two different axial positions on the same side of the acoustic source must be evaluated. The monopole source considered should radiate equally on either side of the source plane. In such cases, the acoustic pressure is continuous across the source but there is a discontinuity in particle velocity [16]. Hence, for a monopole source within a duct, since the modal amplitudes $A_{mn}^{\pm}$ will be equal for all corresponding values of m and n, the general form of $b_{mn}^{\pm}(z)$, for any axial position z in the duct, can be written as [4]

$$b_{mn}^{\pm}(z) = \frac{\psi_{mn}^*(r_s, \theta_s)}{k_{mn}[\tan(\eta_{mn}^{+}(z_s)) - \tan(\eta_{mn}^{-}(z_s))]} \frac{\cos(\eta_{mn}^{\pm}(z))}{\cos(\eta_{mn}^{\pm}(z_s))}. \tag{17}$$

Finally, substitution of Eq. (17) into Eq. (12) shows that the final expression of the Green function for the finite duct is given by

$$G^{\pm}(\mathbf{x}|\mathbf{y}) = \sum_{m=-\infty}^{\infty} \sum_{n=1}^{\infty} \frac{\psi_{mn}(r, \theta)\psi_{mn}^*(r_s, \theta_s)}{k_{mn}[\tan(\eta_{mn}^{+}(z_s)) - \tan(\eta_{mn}^{-}(z_s))]} \frac{\cos(\eta_{mn}^{\pm}(z))}{\cos(\eta_{mn}^{\pm}(z_s))}, \tag{18}$$

where the superscripts $\pm$ refer to the regions, respectively, downstream ($z > z_s$) and upstream ($z < z_s$) of the source ($z = z_s$). This is the case since the axial pressure gradient on either side of the source plane follows from Eq. (16) as different values of $\eta_{mn}^{\pm}(z)$ apply on the two sides (i.e., downstream ($z > z_s$) and upstream ($z < z_s$) of the source).

2.3. The Green function for a semi-infinite cylindrical duct

More realistically, consider the situation depicted in Fig. 2 that corresponds to the case of the experimental fan rig with in which the duct is anechoically terminated on the $+z$ side of the source plane. In Eq. (18), the vanishing of the reflected waves at the end of the $+z$ side implies that the imaginary part of $\eta_{mn}^{+}(z)$ is equal to $-\infty$ (i.e., the reflection coefficient is equal to zero), and hence $\tan(\eta_{mn}^{+}(z_s)) = -j$. The Green function therefore becomes

$$G^{\pm}(\mathbf{x}|\mathbf{y}) = \sum_{m=-\infty}^{\infty} \sum_{n=1}^{\infty} \frac{\psi_{mn}(r, \theta)\psi_{mn}^*(r_s, \theta_s)}{-jk_{mn}[1 - j\tan(\eta_{mn}^{-}(z_s))]} \frac{\cos(\eta_{mn}^{\pm}(z))}{\cos(\eta_{mn}^{\pm}(z_s))}. \tag{19}$$

When measurements are undertaken in the upstream region ($z < z_s$) of the source plane (i.e., sensors are placed between the source plane and the inlet of the duct), the final expression of the

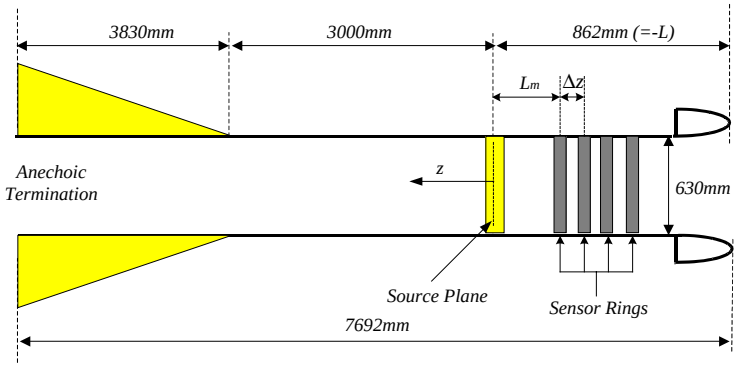

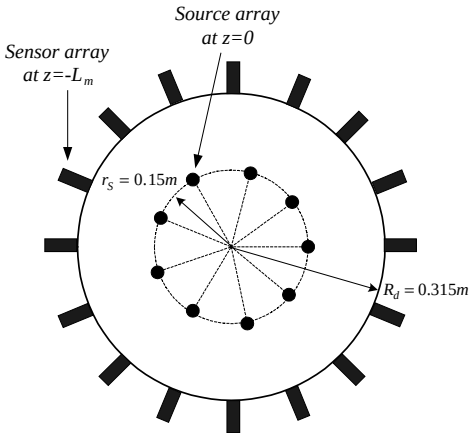

Fig. 2. A geometrical arrangement of the source and sensor array within the semi-infinite cylindrical duct.

Green function for a semi-infinite duct at any axial upstream position z can be written as

$$G(\mathbf{x}|\mathbf{y}) = \sum_{m=-\infty}^{\infty} \sum_{n=1}^{\infty} \frac{\psi_{mn}(r,\theta)\psi^*_{mn}(r_s,\theta_s)}{-\mathrm{j}k_{mn}[1-\mathrm{j}\tan(\eta^-_{mn}(z_s))]} \frac{\cos(\eta^-_{mn}(z))}{\cos(\eta^-_{mn}(z_s))} \quad \text{for } z < z_s. \tag{20}$$

Note that this equation allows the existence of waves in both directions in the upstream region.

2.4. Reflection coefficients

In order to finalize the Green function given by Eq. (20), it is necessary to define the value of $\eta_{mn}(z)$ as a function of the reflection coefficient R_{mn} at the inlet in the duct. Here, the coupling between the incident and the reflected modes is assumed to be neglected at the open end of the duct. Since a particular (m,n) mode will radiate sound mainly through the direct radiation resistance R_{mn} offered by the opening to that mode despite the possibility of coupling with modes of different radial order, the coupling between modes can often be neglected [22]. Thus, the reflection coefficient can be defined in a similar way to that given by Refs. [7,8]. In order to define

this value, use is made of the amplitude ratio at $z = 0$ between the propagating (or incident) and reflected modes presented in Eq. (14). The reflection coefficient at any axial position z in the duct can be written as

$$R^{+}_{mn}(z) = \frac{B^{+}_{mn}\, \mathrm{e}^{-\mathrm{j}k^{-z}_{mn}z}}{A^{+}_{mn}\, \mathrm{e}^{-\mathrm{j}k^{+z}_{mn}z}} = \mathrm{e}^{2\mathrm{j}(\eta^{0+}_{mn}+k_{mn}z)} \quad (z > z_s), \tag{21a}$$

$$\frac{1}{R^{-}_{mn}(z)} = \frac{B^{-}_{mn}\, \mathrm{e}^{-\mathrm{j}k^{-z}_{mn}z}}{A^{-}_{mn}\, \mathrm{e}^{-\mathrm{j}k^{+z}_{mn}z}} = \mathrm{e}^{2\mathrm{j}(\eta^{0-}_{mn}+k_{mn}z)} \quad (z < z_s). \tag{21b}$$

Here, a reflection coefficient at the inlet of the duct (i.e., $z = -L$ as found in Fig. 2) is revealed by setting z equal to $-L$ in Eq. (21b). This is given by

$$R^{-}_{mn}(-L) = \mathrm{e}^{-2\mathrm{j}(\eta^{0-}_{mn}-k_{mn}L)}. \tag{22}$$

This gives

$$\eta^{0-}_{mn} = \frac{-\log R^{-}_{mn}(-L)}{2\mathrm{j}} + k_{mn}L, \tag{23}$$

and therefore the general expression for $\eta_{mn}(z)$ in the final Green function (Eq. (20)) considered at any axial upstream position ($z < z_s$) of the acoustic source can be written as

$$\eta^{-}_{mn}(z) = \frac{-\log R^{-}_{mn}(-L)}{2\mathrm{j}} + k_{mn}(z + L) \quad \text{for } z < z_s. \tag{24}$$

In order to provide a reasonable value of reflection coefficient R_{mn} in Eq. (24), the opening of the duct considered here is assumed to be flangeless. Although a flanged duct can often be an adequate model for determining the sound field inside the duct, a flangeless duct [23] is likely to be a better model for an aircraft engine inlet.

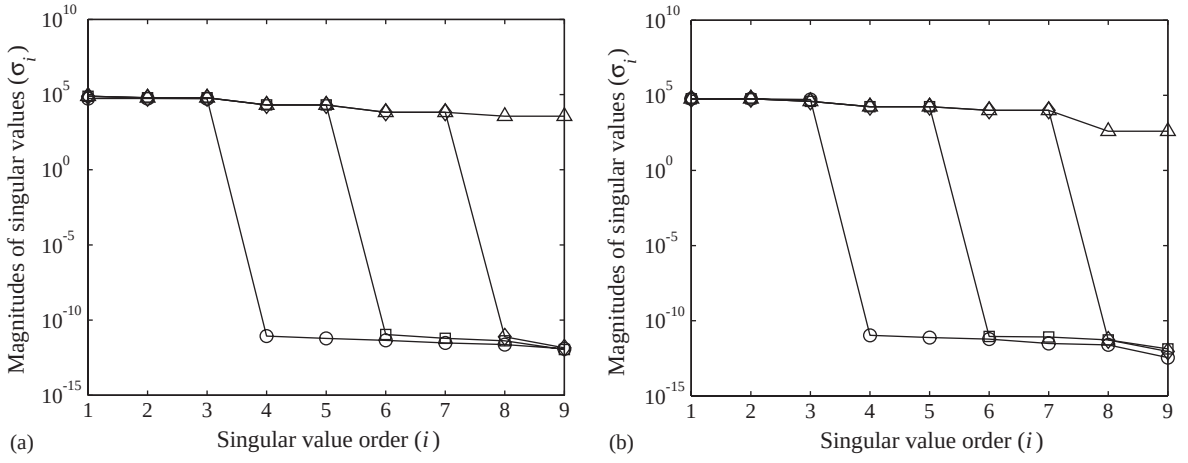

Fig. 3. Magnitude variations of the singular values of the matrix $\mathbf{G}_D$ (nine acoustic sources assumed) with respect to the total number of modes included in calculation of the matrix $\mathbf{G}_D$ for (a) $L_m = -0.1$ m; (b) $L_m = -0.5$ m, when $kR_d = 5$, $N_r = 1$, $N_{s/r} = 9$. Key: —○—, 3 ($m = \pm 1$, $n = 1$); —□—, 10 ($m = \pm 2$, $n = 1$–2); —◇—, 21 ($m = \pm 3$, $n = 1$–3); —△—, 36 ($m = \pm 4$, $n = 1$–4).

In calculating the reflection coefficient R_{mn} for the flangeless duct, the Wiener–Hopf technique [24,25] has been widely used for many years in order to determine the sound reflected into a cylindrical duct when an acoustic spinning mode is propagating toward the open end of the cylindrical duct. However, according to Ref. [26], the most complicated aspect of the Wiener–Hopf technique lies in dealing with complex integrals. The integrals with large parameter values increase the overall computation of the Wiener–Hopf solution, although the numerical complications of the exact solution are not as significant for current computational capabilities. Hence, a simpler approach is desired that can reproduce an accurate representation of the exact solution while reducing the numerical and analytical complexities that arise when using the Wiener–Hopf technique. Therefore, an approximate formula has been introduced as presented recently by Hocter [26]. Briefly, the approach simplifies the complex integral by using the method of steepest descent. Although numerical integration for providing the accurate approximate

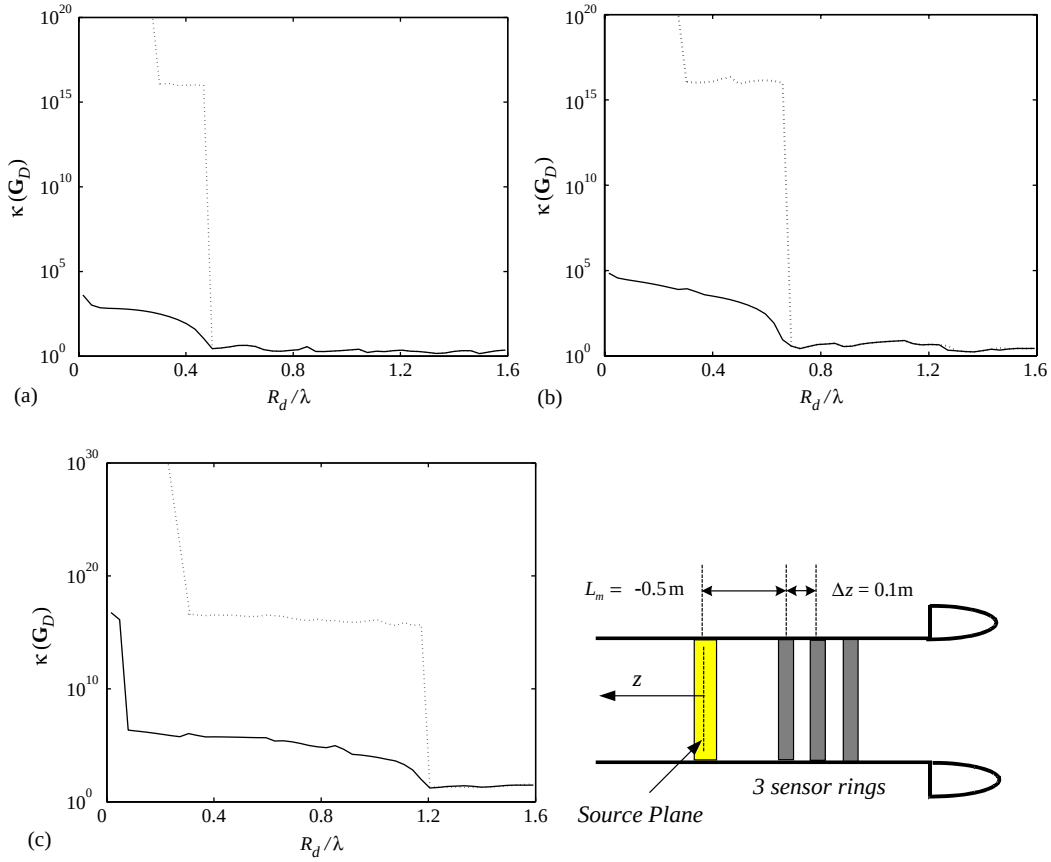

Fig. 4. Comparison of the condition numbers of the matrix $\mathbf{G}_D$ with respect to spinning modes included in calculation of the matrix $\mathbf{G}_D$ (solid line, propagating + evanescent modes; dotted line, evanescent modes), when three sensor rings ($N_r = 3$) are separated by Δz ($=0.1$ m), each containing 16 sensors ($N_{s/r} = 16$), and the closest ring from the acoustic sources is located at $L_m = -0.5$ m for (a) five acoustic sources assumed, (b) seven acoustic sources assumed, (c) 12 acoustic sources assumed.

solution of the exact Wiener–Hopf solution is still required, it is significantly less complicated than the exact solution. Details of practical applications have been presented in references [4,26,27]. Therefore, the general expression of $\eta_{mn}(z)$, Eq. (24), at any axial upstream position ($z < z_s$) of the acoustic source can be estimated by using this approximate formula.

3. Conditioning of the frequency response function matrix for the duct acoustic model

Consider the hard-walled semi-infinite duct depicted in Fig. 2, where the source is simply assumed to consist of a number of point monopole sources. The M discrete acoustic pressures in the upstream region of the duct are related to the N discrete source strengths via the frequency response functions. These are written in matrix form:

$$\mathbf{G}_D = \begin{bmatrix} G(x_1|y_1) & G(x_1|y_2) & \cdots & \cdots & G(x_1|y_N) \\ G(x_2|y_1) & G(x_2|y_2) & \cdots & \cdots & G(x_2|y_N) \\ \cdots & \cdots & \cdots & \cdots & \cdots \\ \cdots & \cdots & \cdots & \cdots & \cdots \\ G(x_M|y_1) & G(x_M|y_2) & \cdots & \cdots & G(x_M|y_N) \end{bmatrix}, \tag{25}$$

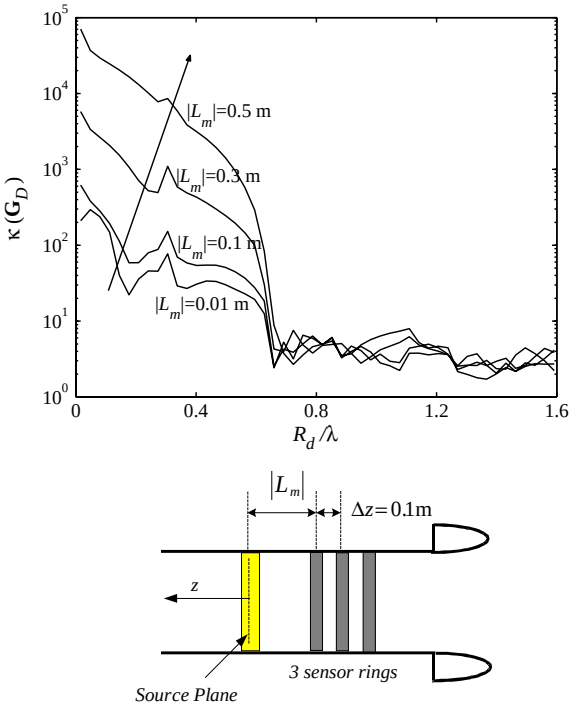

Fig. 5. Variations of the condition number $\kappa(\mathbf{G}_D)$ (for seven acoustic sources assumed) with respect to the axial separation $|L_m|$, when three sensor rings ($N_r = 3$) are separated by Δz ($= 0.1$ m), each containing 16 sensors ($N_{s/r} = 16$).

where each element $G(x_M|y_N)$ obtained from Eq. (20) is the Green function between measured pressure at discrete field point x_M and a point source at y_N.

In order to illustrate the main factors affecting the conditioning of the matrix $\mathbf{G}_D$, an assumed geometrical arrangement of sensors and sources within the duct depicted in Fig. 2 has been used. Here, it is assumed that nine radiating point monopole sources at the axial position $z = 0$ are placed at the radial distance from the centre of the duct (i.e., $r_s = 0.15\,\mathrm{m} = 0.48R_d$) at equal circumferential increments. The sensor array is comprised of a number of rings, N_r with a separation distance between them of Δz. Here, each ring contains a certain number of sensors, $N_{s/r}$, and the sensors are mounted flush on the duct wall. The closest of the sensor rings to the source plane is located at $z = -L_m$.

Firstly, for illustrative purposes, the measurements are assumed to be undertaken by only the single ring at a frequency corresponding to $kR_d = 5$. Fig. 3 shows magnitude variations of singular values in the frequency response function matrix $\mathbf{G}_D$ to be inverted with respect to the total number of modes included in calculation of the matrix. In this figure, as the total number of modes considered increases, the singular values σ_i decay gradually and continuously. However, when only a small number of the modes are included in the calculation of the matrix $\mathbf{G}_D$, the distribution of the singular values includes a sudden jump in value, and thus the condition number of the matrix $\mathbf{G}_D$ becomes much higher than that when a large number of modes are included.

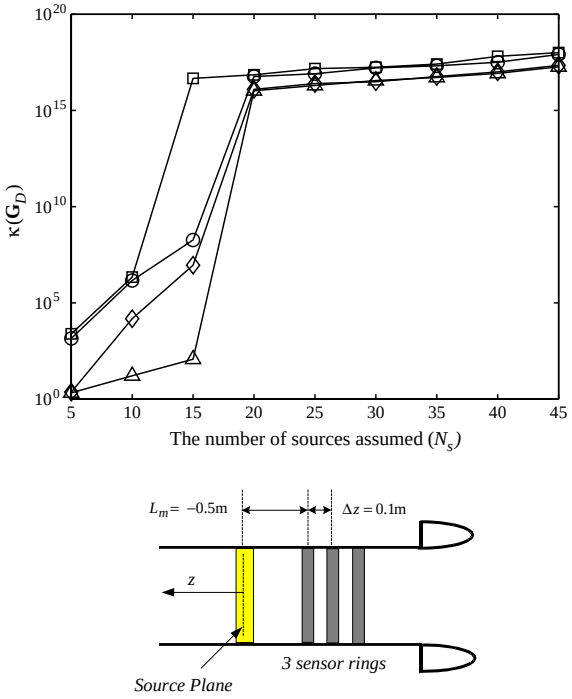

Fig. 6. Variations of the condition number $\kappa(\mathbf{G}_D)$ with respect to the different number of acoustic sources assumed, when three sensor rings ($N_r = 3$) are separated by Δz ($= 0.1$ m), each containing 16 sensors ($N_{s/r} = 16$), and the closest ring from the acoustic sources is located at $L_m = -0.5$ m. Key: —○—, $kR = 0.5$; —□—, $kR = 1.0$; —◇—, $kR = 5.0$; —△—, $kR = 10.0$.

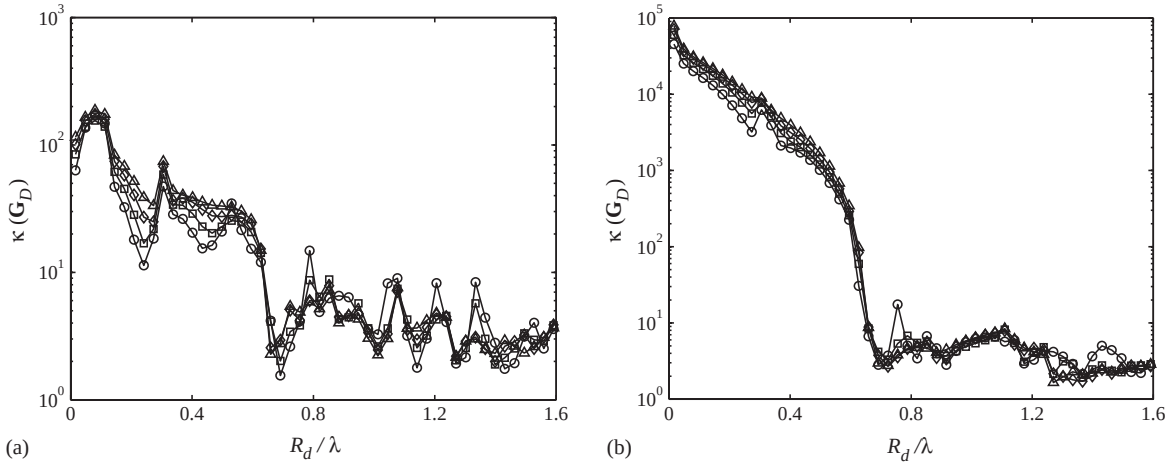

Fig. 7. Variations of the condition number $\kappa(\mathbf{G}_D)$ (for seven acoustic sources assumed) with respect to different configurations of the sensor rings for (a) $L_m = -0.01$ m, (b) $L_m = -0.5$ m, when the total number of the sensors is 48 and the sensor rings are separated by Δz ($=0.1$ m). Key: —○—, $N_r = 1$, $N_{s/r} = 48$; —□—, $N_r = 2$, $N_{s/r} = 24$; —◇—, $N_r = 3$, $N_{s/r} = 16$; —△—, $N_r = 4$, $N_{s/r} = 12$.

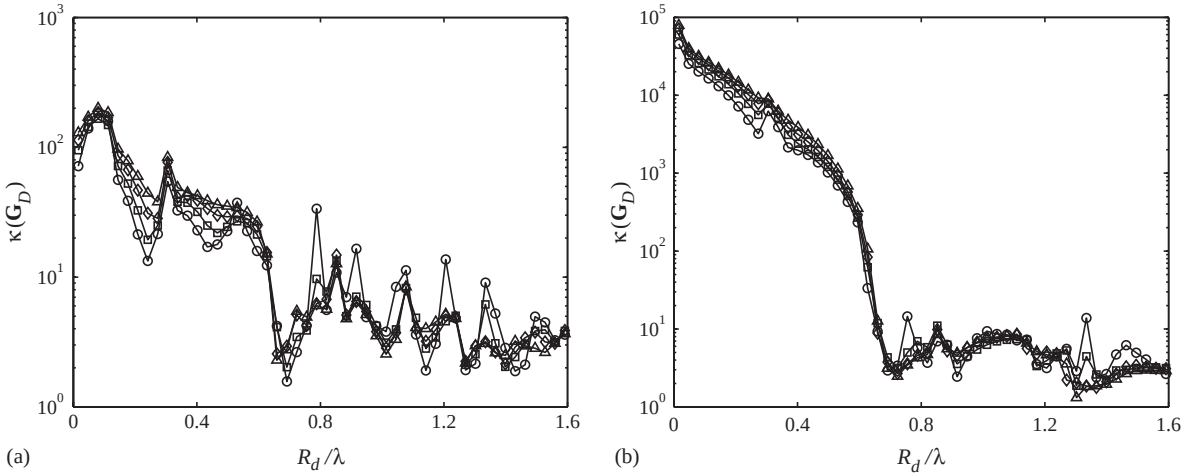

Fig. 8. Variations of the condition number $\kappa(\mathbf{G}_D)$ (for seven acoustic sources assumed) with respect to different configurations of the sensor rings for (a) $L_m = -0.01$ m, (b) $L_m = -0.5$ m, when the sensor rings are separated by Δz ($=0.1$ m), each containing eight sensors ($N_{s/r} = 8$). Key: —○—, $N_r = 1$, $N_{s/r} = 8$; —□—, $N_r = 2$, $N_{s/r} = 8$; —◇—, $N_r = 3$, $N_{s/r} = 8$; —△—, $N_r = 4$, $N_{s/r} = 8$.

Therefore, in order to reduce the condition number $\kappa(\mathbf{G}_D)$, it seems to be necessary to consider cut-off modes (i.e., evanescent modes).

In order to better illustrate this point, consider a multi-ring sensor array, since it often is impractical to use only a single ring for a large number of sensors. For example, as depicted in

Fig. 4, the multi-ring sensor array is assumed to have three rings ($N_r = 3$) separated by a distance $\Delta z = 0.1$ m apart, each containing 16 sensors ($N_{s/r} = 16$), and the closest ring from the acoustic sources is located at $L_m = -0.5$ m. As shown in Fig. 4, when the evanescent modes as well as the propagating modes are included in calculation of the matrix $\mathbf{G}_D$, it is clearly found that the conditioning of the matrix is much improved in the range of small non-dimensional frequencies below a certain frequency. The critical frequency is higher as the number of the assumed acoustic sources increases. However, if only propagating modes are considered, the condition number $\kappa(\mathbf{G}_D)$ of the matrix $\mathbf{G}_D$ is suddenly increased at the cut-off frequency. This represents clear evidence that in order to reduce the sensitivity to various kinds of errors, the evanescent modes must be considered. This may be very helpful in increasing the spatial resolution of the source reconstruction process. Otherwise, the condition number $\kappa(\mathbf{G}_D)$ of the matrix $\mathbf{G}_D$ becomes large and poor conditioning will result in the amplification of any errors, particularly in the relatively low non-dimensional frequency range. Note that the desirability of sensing evanescent modes is in contrast to that associated with the active control problem [28,29].

The most important parameter to be expected to have a crucial influence on the conditioning of the matrix $\mathbf{G}_D$ is thus the axial distance between the source plane and the sensor plane. As shown in Fig. 5, as the axial separation $|L_m|$ between the source and measurement positions is increased, the conditioning of the matrix $\mathbf{G}_D$ to be inverted becomes worse, particularly at low values of R_d/λ. Whereas, at relatively high values of R_d/λ (for example when R_d/λ is bigger than 0.63 approximately which is the non-dimensional cut-off frequency in the case investigated), the conditioning of the matrix $\mathbf{G}_D$ is insensitive to the axial distance between the source and the measurement positions. Thus, in order to capture the evanescent modes associated with high spatial frequencies, measurements must be undertaken in the field close to the acoustic source

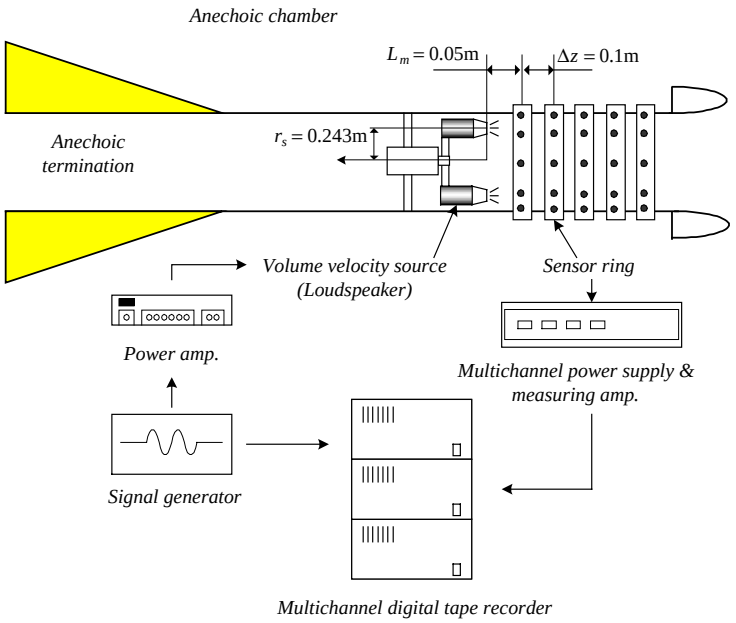

Fig. 9. Arrangement of the experimental rig.

Fig. 10. A picture of the experimental rig in the ISVR anechoic chamber.

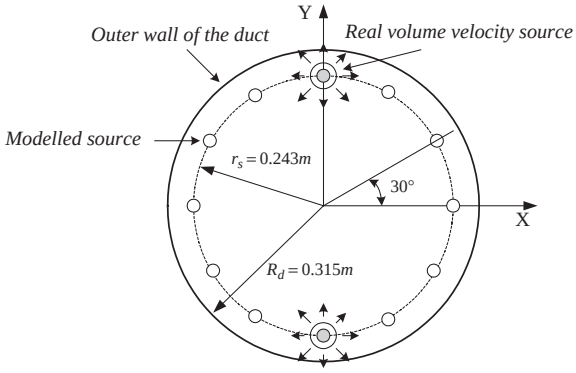

Fig. 11. A schematic diagram for the modelled sources and the real volume velocity sources mounted inside the duct.

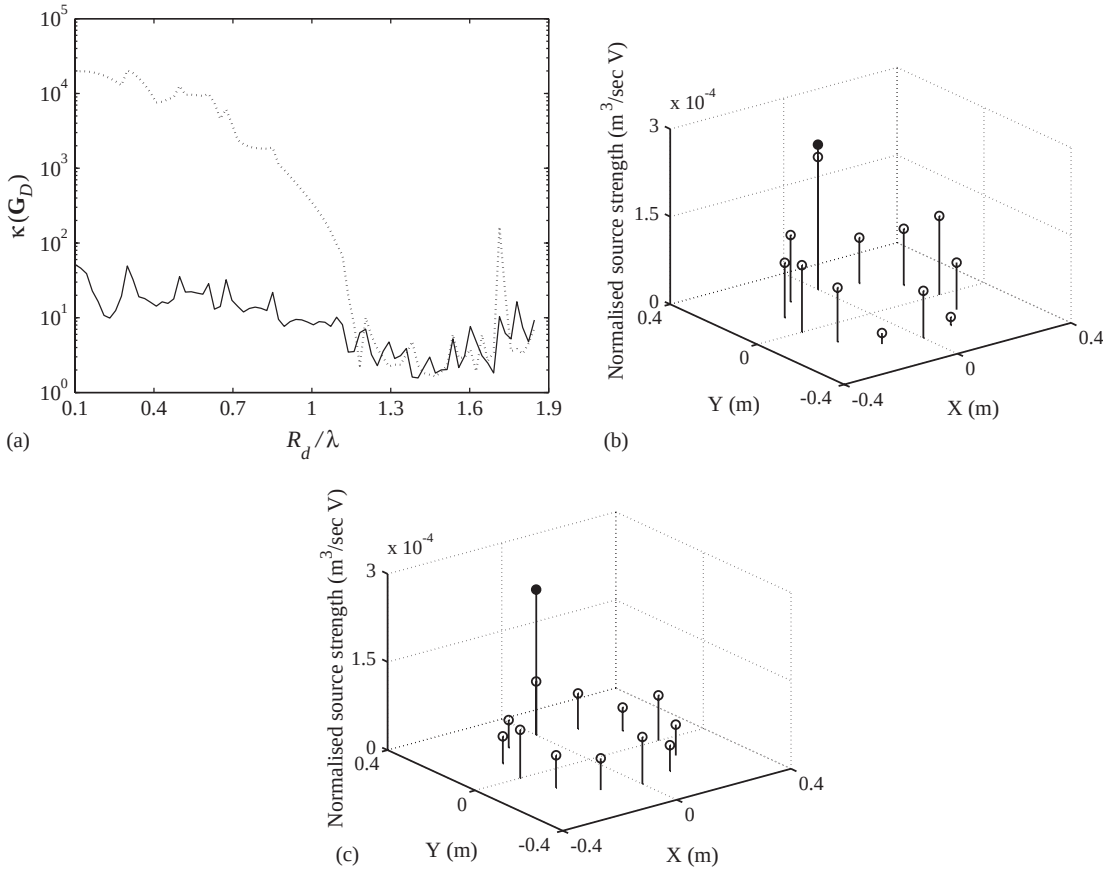

Fig. 12. Comparison of the reconstruction results with respect to the axial separation $|L_m|$, when the radiated field is generated by one real acoustic source of 12 model sources. The sound field is measured with one sensor ring ($N_r = 1$) containing 12 sensors ($N_{s/r} = 12$). (a) Comparison of the condition numbers of the matrices $\mathbf{G}_D$ (solid line, $|L_m| = 0.05$ m; dotted line, $|L_m| = 0.35$ m). (b) Reconstruction result produced by Tikhonov regularization with β_{GCV}, when $R_d/\lambda = 0.54$ and $|L_m| = 0.05$ m (•, true; ◦, reconstructed). (c) Reconstruction result produced by Tikhonov regularization with β_{GCV}, when $R_d/\lambda = 0.54$ and $|L_m| = 0.35$ m (•, true; ◦, reconstructed).

plane. This is exactly consistent with the known behaviour of planar NAH described in Ref. [20]. Therefore, the resolution and the accuracy of the reconstruction of in-duct source distribution may also be highly dependent on how these small singular values associated with the evanescent modes are treated during the inversion process.

Another factor affecting the conditioning of the matrix $\mathbf{G}_D$ to be considered is the assumed number of model sources and number of measurement positions. Firstly, as illustrated in Fig. 6, the matrix $\mathbf{G}_D$ to be inverted tends to become more ill-conditioned as the number of the assumed acoustic sources increases. As might be expected, when the number of the acoustic sources assumed becomes larger than the number of sensors per ring $N_{s/r}$ (in this case, $N_{s/r} = 16$), the condition number $\kappa(\mathbf{G}_D)$ of the matrix $\mathbf{G}_D$ suddenly increases in magnitude. The number of measurement positions is therefore subject to the constraint that $N_{s/r}$ is more than at least the

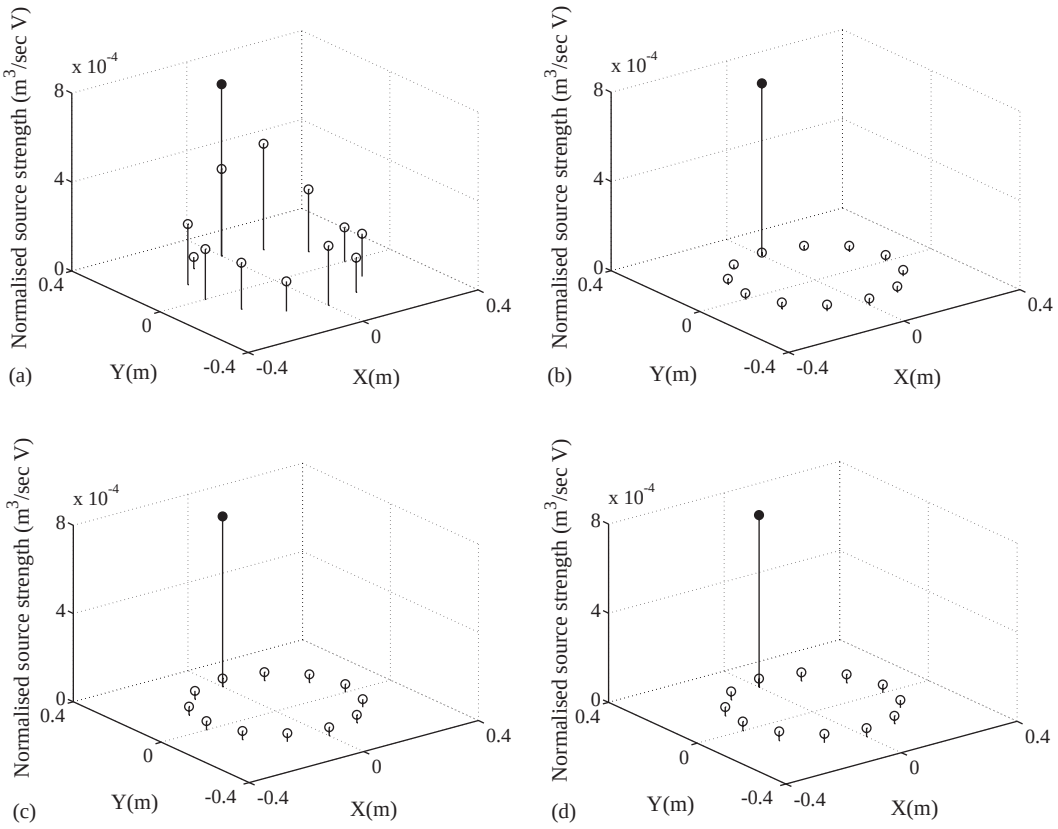

Fig. 13. Reconstruction results (•, true; ◦, reconstructed), when the radiated field is generated by one real acoustic source of 12 model sources and $R_d/\lambda = 0.1$ (106 Hz). The sound field is measured with one sensor ring ($N_r = 1$) containing 12 sensors ($N_{s/r} = 12$) when (a) $L_m = -0.05$ m and $\beta = \beta_{GCV}$; (b) $L_m = -0.05$ m and $\beta = \beta_{LCV}$; (c) $L_m = -0.35$ m and $\beta = \beta_{GCV}$; (d) $L_m = -0.35$ m and $\beta = \beta_{LCV}$.

assumed number of the acoustic sources N_s. As shown in Fig. 7, when the equivalent number of sensors is used, very similar variation of the condition number $\kappa(\mathbf{G}_D)$ is exhibited even for different configurations of the wall-mounted sensors in the form of a number of sensor rings uniformly distributed along the length of the intake duct. Also, even when the sensor array is close to the assumed source plane, very similar results are produced. As illustrated in Fig. 8, the conditioning of the matrix $\mathbf{G}_D$ seems to be insensitive to the number of sensor rings N_r when each ring contains at least the same number of sensors per ring as that of the assumed sources.

4. Experimental verification of the reconstruction of in-duct acoustic source strength

4.1. Experimental system

The work presented in the previous section has shown that the inverse technique may still be useful for dealing with in-duct sound source problems, since the exponentially decaying cut-off

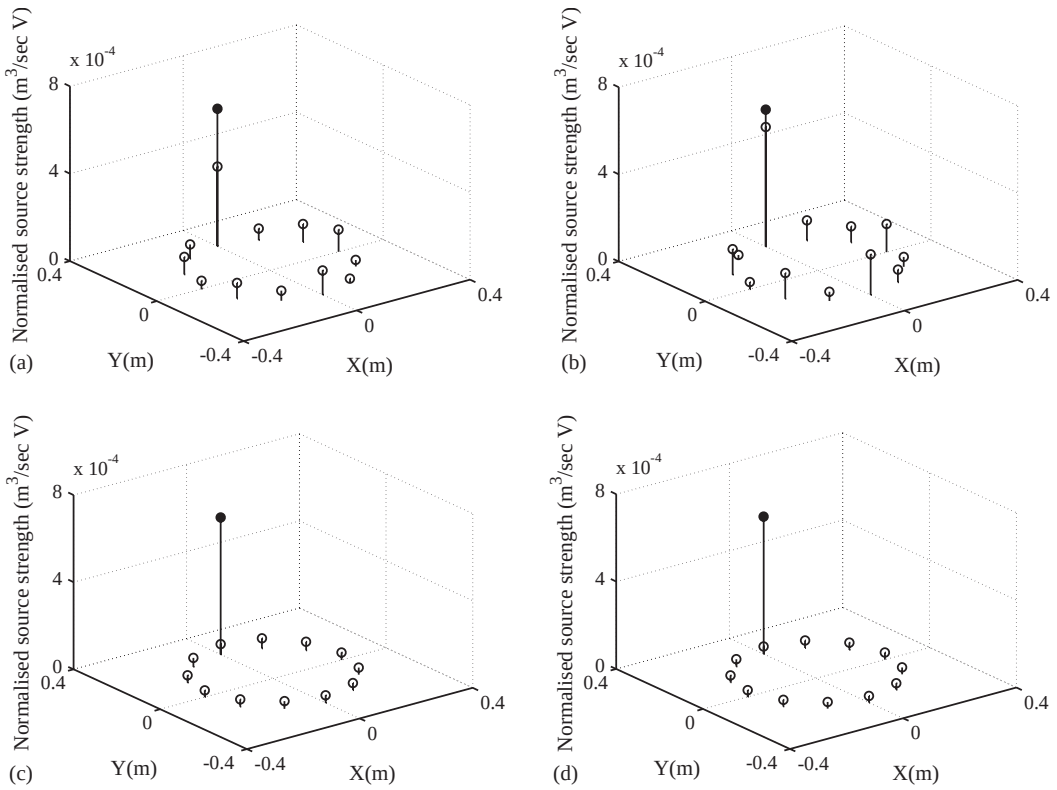

Fig. 14. Reconstruction results (•, true; ◦, reconstructed), when the radiated field is generated by one real acoustic source of 12 model sources and $R_d/\lambda = 0.15$ (159 Hz). The sound field is measured with one sensor ring ($N_r = 1$) containing 12 sensors ($N_{s/r} = 12$) when (a) $L_m = -0.05$ m and $\beta = \beta_{GCV}$; (b) $L_m = -0.05$ m and $\beta = \beta_{LCV}$; (c) $L_m = -0.35$ m and $\beta = \beta_{GCV}$; (d) $L_m = -0.35$ m and $\beta = \beta_{LCV}$.

modes which contain high-resolution information about the acoustic sources are associated with the small singular values of the matrix $\mathbf{G}_D$. It has been shown through the numerical simulations presented that measurements should be undertaken in the near field of the acoustic source in order to capture the evanescent modes. This should enable the production of greater spatial resolution of the source distribution. It therefore is useful to show a practical demonstration of these results and to see how the inverse technique considered here works in practical applications.

The experiments described below make use of a fan test rig, which consists of a ducted fan with a low distortion inlet and an anechoic outlet as depicted in Figs. 9 and 10 (the outline dimensions of the fan rig are shown in Fig. 2). Here, instead of the ducted fan, 12 volume velocity sources are assumed to be evenly distributed at $r_s = 0.243$ m. This is illustrated in Fig. 11. Real volume velocity sources of 12 model sources generate the sound field inside the duct, where two small loudspeakers are mounted on the same axial position as the inducted fan. The details of the real sources, such as their locations and strengths are assumed unknown and thus it is assumed that there are 12 model sources. The loudspeakers are driven individually by complete different random signals which cover all frequencies within the bandwidth of the measurement system. The

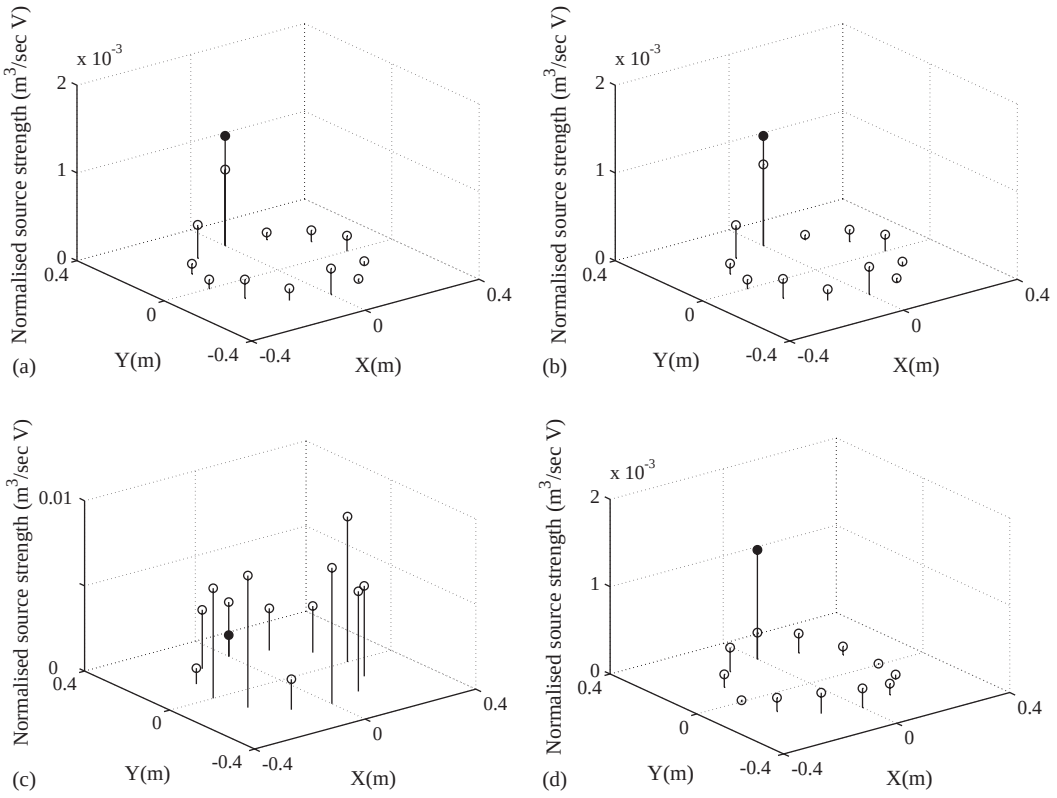

Fig. 15. Reconstruction results (•, true; ◦, reconstructed), when the radiated field is generated by one real acoustic source of 12 model sources and $R_d/\lambda = 0.25$ (270 Hz). The sound field is measured with one sensor ring ($N_r = 1$) containing 12 sensors ($N_{s/r} = 12$) when (a) $L_m = -0.05$ m and $\beta = \beta_{GCV}$; (b) $L_m = -0.05$ m and $\beta = \beta_{LCV}$; (c) $L_m = -0.35$ m and $\beta = \beta_{GCV}$; (d) $L_m = -0.35$ m and $\beta = \beta_{LCV}$.

source strength of each real source was calibrated by the farfield acoustic pressures which is measured by sensors at a known distance away from the sources, and the calibration process is described in Ref. [4]. The calibrated real sources are individually driven by random signals and their details such as locations and volume velocities are assumed to be unknown.

The sensor array depicted in Fig. 9 consists of five rings separated by distance $\Delta z = 0.1$ m and each ring supports a maximum of 24 sensors (i.e., $N_{s/r} = 24$) mounted flush on the duct wall parallel to the cross-section. The measured field data and the input signals for driving the loudspeakers are simultaneously stored through multi-channel digital tape recorder as shown in Fig. 9. All the electret microphones used were calibrated in situ because the sensitivity of the microphone may be changed by its mounted condition.

4.2. Reconstruction of volume velocity sources using experimental data

For experimental reconstruction of the volume velocity source distribution within the duct, measurements of internal acoustic pressures have been undertaken with the experimental

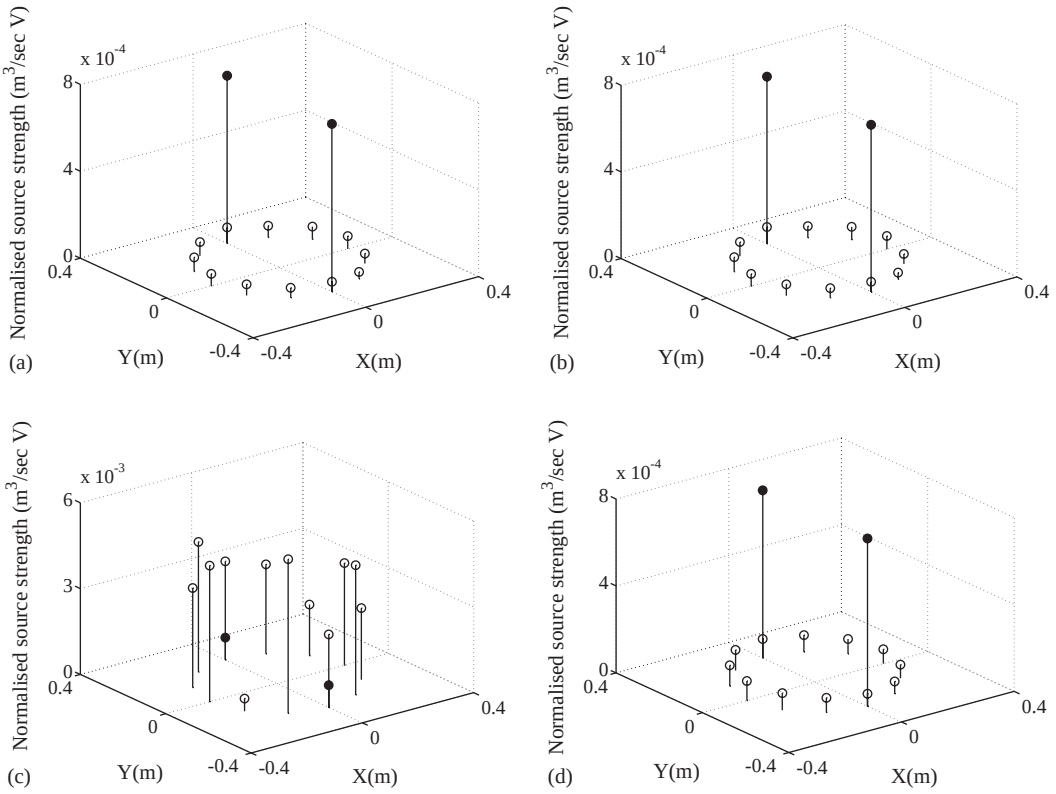

Fig. 16. Reconstruction results (•, true; ◦, reconstructed), when the radiated field is generated by two real acoustic source of 12 model sources and $R_d/\lambda = 0.1$ (106 Hz). The sound field is measured with one sensor ring ($N_r = 1$) containing 12 sensors ($N_{s/r} = 12$) when (a) $L_m = -0.05$ m and $\beta = \beta_{GCV}$; (b) $L_m = -0.05$ m and $\beta = \beta_{LCV}$; (c) $L_m = -0.35$ m and $\beta = \beta_{GCV}$; (d) $L_m = -0.35$ m and $\beta = \beta_{LCV}$.

system illustrated in Figs. 9 and 10. In the experimental process, the theoretical Green function given by Eq. (20) has been used for the frequency response relations between the internal pressures and the assumed source distribution within the duct. In this section, the results of a series of reconstructions using the experimental data are presented, and some practical considerations are addressed of the regularization parameter-determination methods (i.e., GCV and the L-curve method).

As observed from the results simulated in the previous section, it is easily recognized that the essence of the successful reconstruction of acoustic source distribution lies in keeping the condition number as small as possible by adjusting the geometrical arrangement of discretized model sources and sensors. Therefore, it is valuable to examine the main factor affecting the conditioning of the matrix $\mathbf{G}_D$ described in Section 3 for the practical case investigated here, even though it is not straightforward to express quantitatively the boundary of large and small condition numbers. Fig. 12 shows the effect of the axial separation $|L_m|$ between the source plane and the sensor plane on the reconstruction results with the experimental cases investigated, when only one real source of 12 model sources depicted in Fig. 11 generates the

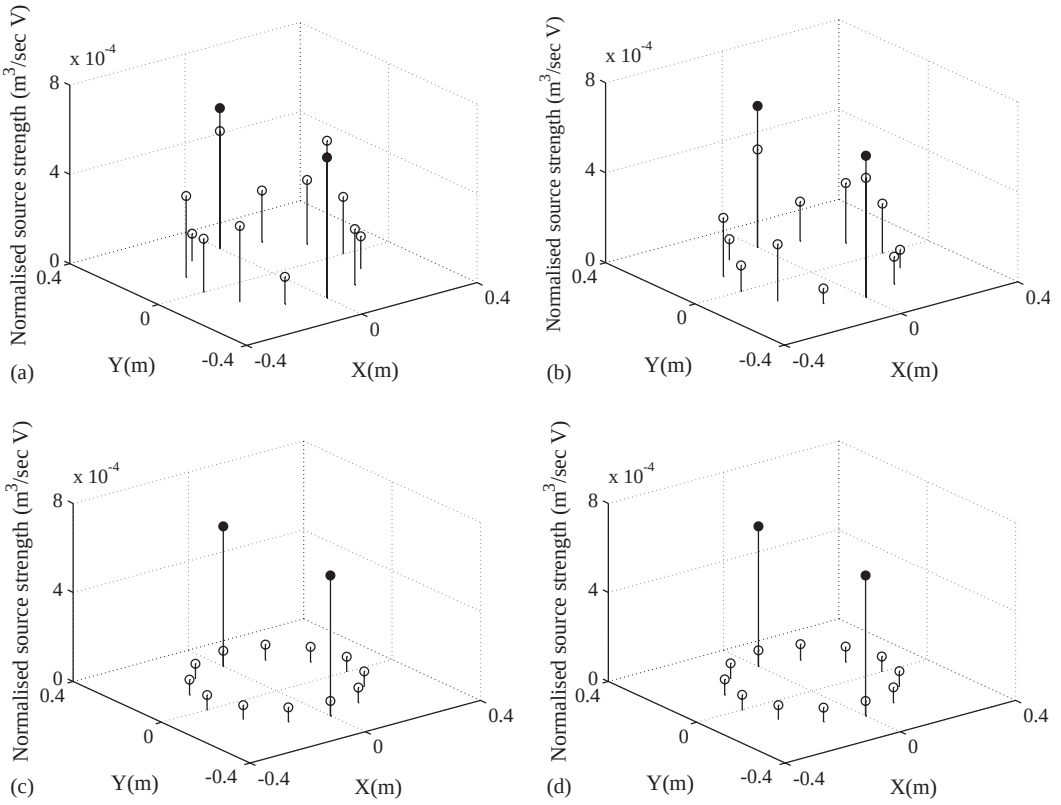

Fig. 17. Reconstruction results (•, true; ◦, reconstructed), when the radiated field is generated by two real acoustic source of 12 model sources and $R_d/\lambda = 0.15$ (159 Hz). The sound field is measured with one sensor ring ($N_r = 1$) containing 12 sensors ($N_{s/r} = 12$) when (a) $L_m = -0.05$ and $\beta = \beta_{GCV}$; (b) $L_m = -0.05$ m and $\beta = \beta_{LCV}$; (c) $L_m = -0.35$ m and $\beta = \beta_{GCV}$; (d) $L_m = -0.35$ m and $\beta = \beta_{LCV}$.

sound radiated field. Note that the reconstructed source distribution is provided by Tikhonov regularization. For the real source, the calibrated loudspeaker is used and thus the strength of the real source is known. In Fig. 12(a), the better conditioning of the matrix $\mathbf{G}_D$ is exhibited as the sensor plane is close to the acoustic sources, particularly in the region of small R_d/λ. The results of the reconstruction of the acoustic source distribution are shown in Fig. 12(b) for $|L_m| = 0.05$ m and it is clear that a better reconstruction is produced compared with that shown in Fig. 12(c) for $|L_m| = 0.35$ m.

Figs. 13–15 show the real and experimentally reconstructed source distributions with GCV and the L-curve method with one ring sensor array ($N_r = 1$)) which contains 12 sensors ($N_{s/r} = 12$) and which is located at $L_m = -0.05$ m (which is the closest position from the sources in the experimental models). The radiated sound field is generated by only one unknown source of 12 assumed sources. Firstly, at $R_d/\lambda = 0.1$ (106 Hz) shown in Fig. 13, the real source location cannot be distinguished at all, even when the acoustic pressures measured are regularized with the regularization parameters, β_{GCV} provided by GCV and β_{LCV} provided by the L-curve method, during the inversion processes. Furthermore, the

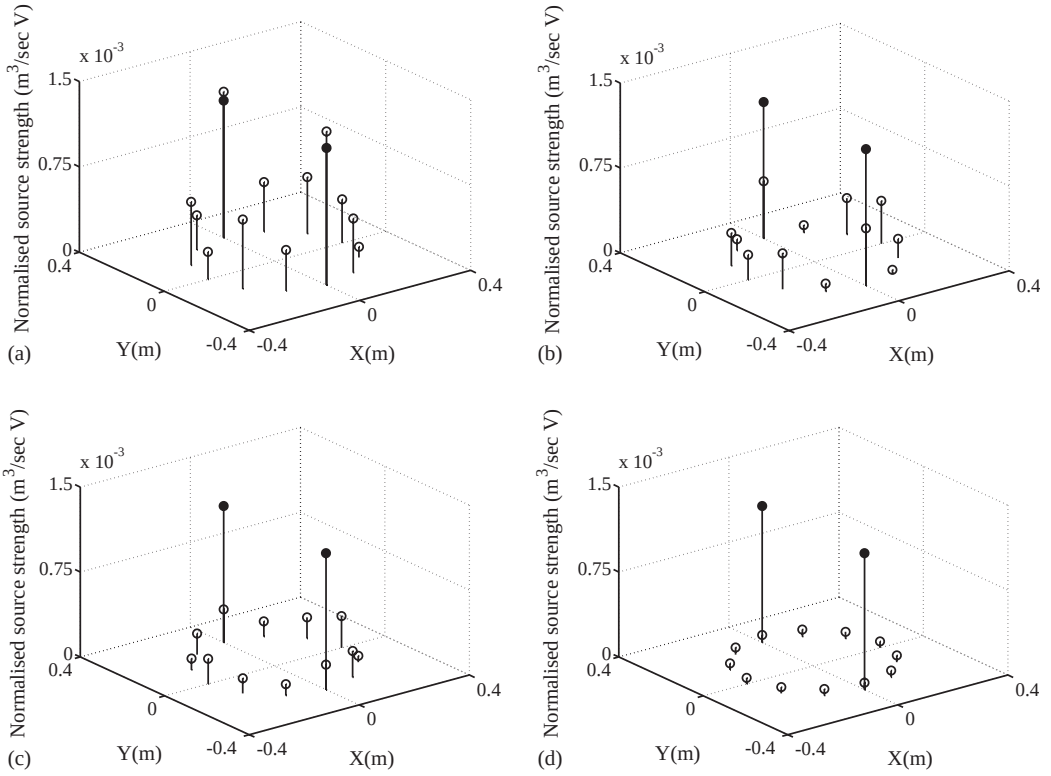

Fig. 18. Reconstruction results (•, true; ◦, reconstructed), when the radiated field is generated by two real acoustic source of 12 model sources and $R_d/\lambda = 0.25$ (270 Hz). The sound field is measured with one sensor ring ($N_r = 1$) containing 12 sensors ($N_{s/r} = 12$) when (a) $L_m = -0.05$ and $\beta = \beta_{GCV}$; (b) $L_m = -0.05$ m and $\beta = \beta_{LCV}$; (c) $L_m = -0.35$ m and $\beta = \beta_{GCV}$; (d) $L_m = -0.35$ m and $\beta = \beta_{LCV}$.

magnitudes of the reconstructed results are very inaccurate compared with the true source strength.

However, when $R_d/\lambda = 0.15$ (159 Hz), as shown in Fig. 14, the closest sensor array from the acoustic sources can reveal exactly the location of the unknown real source by the application of Tikhonov regularization. Here, the L-curve method can accurately reconstruct the strength of the unknown source. In the case investigated, the L-curve method provides more a reasonable regularization parameter than GCV. When $R_d/\lambda = 0.25$ (270 Hz) in Fig. 15, the real source can be distinguished clearly with reasonable accuracy by the use of Tikhonov regularization.

When the radiated sound field is generated by two unknown real sources, it is interesting to see whether the sensor array can still be effective in providing high-resolution estimation of the strengths of the unknown real sources. Figs. 16–18 demonstrate very similar resolution limits for the reconstruction of the acoustic source strength distribution, even when two real sources are operating. In other words, similarly to the cases for one unknown real source, better spatial resolution can be seen as the sensor array is placed close to the acoustic sources.

5. Conclusions

In this paper, an analytical model has been used for the internal field of a semi-infinite duct with an open end. The internal acoustic field generated by a source within the circular duct can be constructed from an infinite series of modes, which are partially reflected at the end of the duct. This analytical model, which offers great potential flexibility in dealing with this kind of the problem, has been used to examine practically the capability of the inverse technique considered. Initially, using the analytical model, it has been demonstrated by means of the SVD that ill-conditioning is usually provided by the small singular values of the matrix $\mathbf{G}_D$ in in-duct sound source problems. It has been shown that the small singular values in the matrix $\mathbf{G}_D$ are associated with evanescent modes containing high spatial frequency information associated with the acoustic source distribution. These are very similar to the results of the SVD analysis used for investigating the spatial resolution of reconstructed source images in freefield radiation. As a result of numerical simulations, it has been shown that the ill-conditioning of the matrix $\mathbf{G}_D$ can be overcome by consideration of evanescent modes within the duct and thus measurements must be undertaken in the field close to the acoustic sources. Also, for the case investigated here, it has been shown that the conditioning of the matrix $\mathbf{G}_D$ can be much improved when a relatively small number of sources is assumed. Results have been presented of practical investigations of the abilities of two different regularization parameter-determination methods (GCV and the L-curve method). Through a series of experimental reconstructions, it has been demonstrated that greater spatial resolution of the acoustic source distribution can be realized by the use of measurements undertaken close to the sources.

References

[1] Y. Kim, P.A. Nelson, Regularisation methods for acoustic source reconstruction, *Proceedings of InterNoise 2000*, Vol. 1, 2000, pp. 128–132.
[2] P.A. Nelson, A review of some inverse problems in acoustics, *International Journal of Acoustics and Vibration* 6 (3) (2001) 118–134.
[3] Y. Kim, P.A. Nelson, Spatial resolution limits for the reconstruction of acoustic source strength by inverse method, *Journal of Sound and Vibration* 265 (2003) 583–608.
[4] Y. Kim, Spatial Resolution Limits for the Reconstruction of Acoustic Source Distribution by Inverse Techniques, Ph.D. Thesis, University of Southampton, 2002.
[5] B.D. Mugridge, C.L. Morfey, Sources of noise in axial flow fans, *Journal of the Acoustical Society of America* 51 (1972) 1411–1426.
[6] M.E. Goldstein, *Aeroacoustics,*, McGraw-Hill, New York, 1976.
[7] C.L. Morfey, Rotating pressure patterns in ducts: their generation and transmission, *Journal of Sound and Vibration* 1 (1964) 60–87.
[8] C.L. Morfey, Sound transmission and generation in ducts with flow, *Journal of Sound and Vibration* 14 (1) (1971) 37–55.
[9] J.M. Tyler, T.G. Sofrin, Axial flow compressor noise studies, *SAE Transactions* 70 (1962) 309–332.
[10] A.N. Tikhonov, Solution of incorrectly formulated problems and the regularization method, *Soviet Mathematics Doklady* 4 (1963) 1035–1038.
[11] A.N. Tikhonov, V.Y. Arsenin, *Solutions of Ill-posed Problems*, Winston, Washington, DC, 1977.
[12] G.H. Goulb, M. Health, G. Wahba, Generalised cross-validation as a method for choosing a good ridge parameter, *Technometrices* 21 (1979) 215–223.

[13] G. Wahba, *Spline Models for Observation Data*, CBMS-NSF Regional Conference Series in Applied Mathematics, SIAM, Philadelphia, 1990.
[14] P.C. Hansen, Analysis of discrete ill-posed problems by means of the L-curve, *SIAM Review* 34 (1992) 561–580.
[15] P.C. Hansen, D.P. O'Leary, The use of the L-curve in the regularization of discrete ill-posed problem, *SIAM Journal on Science and Computing* 14 (1993) 1487–1503.
[16] D.A.K. Hewlett, The Radiation from Acoustic Sources within a Finite Length Circular Duct Immersed in Water, Ph.D. Thesis, University of Southampton, 1995.
[17] E.G. Williams, *Fourier Acoustics: Sound Radiation and Nearfield Acoustical Holography*, Academic Press, London, 1999.
[18] J.D. Maynard, E.G. Williams, Y. Lee, Nearfield acoustic holography: I. theory of generalised holography and the development of NAH, *Journal of the Acoustical Society of America* 78 (4) (1985) 1395–1413.
[19] W.A. Veronesi, J.D. Maynard, Digital holographic reconstruction of sources with arbitrarily shaped surfaces, *Journal of the Acoustical Society of America* 85 (2) (1989) 588–598.
[20] E.G. Williams, B.H. Huston, P.C. Herdic, Reconstruction of the surface velocity and interior acoustic intensity from an aircraft fuselage using nearfield acoustical holography, *Proceedings of Noise-Control* 96, 1996, pp. 193–198.
[21] D.A.K. Hewlett, P.A. Nelson, A model based approach for estimating the strength of acoustic sources within a circular duct, *Second AIAA/CEAS Aeroacoustics Conference*, State College, PA, 1996.
[22] C.L. Morfey, A note on the radiation efficiency of acoustic duct modes, *Journal of Sound and Vibration* 9 (3) (1969) 367–372.
[23] W.E. Zorumski, Generalised radiation impedances and reflection coefficients of circular and annular ducts, *Journal of the Acoustical Society of America* 54 (1973) 1667–1673.
[24] L.A. Weinstein, *Open Resonators and Open Waveguides*, Golem, Boulder, CO, 1969.
[25] L.A. Weinstein, *The Theory of Diffraction and the Factorisation Method (Generalized Wiener–Hopf Technique)*, Golem, Boulder, CO, 1969.
[26] S.T. Hocter, Sound reflection into a cylindrical duct, *Proceedings of the Royal Society of London, Series A* 456 (2000) 2707–2716.
[27] C. Pitelet, Flow Control for Fan Noise Reduction, M.Sc. Dissertation, University of Southampton, 2000.
[28] P. Joseph, E.F. Fruteau, P.A. Nelson, Design rules and sensing strategies for the active control of turbofan engine noise, *7th AIAA/CEAS Aeroacoustics Conference*, Maastricht, Netherlands, 2001, pp. 2001–2222.
[29] P. Joseph, P.A. Nelson, M.J. Fisher, Active control of fan tones radiated from turbofan engines, II In-duct error sensors, *Journal of the Acoustical Society of America* 106 (1999) 779–786.